Origin of Stokes shift in InAs and CdSe quantum dots: Exchange splitting of excitonic states

Anjana Bagga,[1] P. K. Chattopadhyay,[2] and Subhasis Ghosh[1]
[1]*School of Physical Sciences, Jawaharlal Nehru University, New Delhi 110067, India*
[2]*Department of Physics, Maharshi Dayanand University, Rohtak, India*
(Received 21 April 2006; published 28 July 2006)

The mechanism of Stokes shift in semiconductor quantum dots is investigated by calculating the energy of the excitonic states. We have taken into account all possible contributions to the total electronic energy in the dot—i.e., the dielectric mismatch between the dot and surrounding medium, the effects of finite barrier height, and the electron-hole exchange interaction. The Stokes shift is calculated as a function of radius of dot and compared with experimental data on two different semiconductor based quantum dots. These results provide evidence for an exchange splitting of excitonic states, as the mechanism of Stokes shift in quantum dots.

DOI: 10.1103/PhysRevB.74.035341 PACS number(s): 73.21.La, 73.22.−f, 72.80.Ey

I. INTRODUCTION

The redshift of the emission spectra with respect to absorption spectra is known as Stokes shift, which is commonly observed in semiconductor quantum dots (QD's) and is one of the most important quantities that determine the optical properties of QD's. Several observations of Stokes shift and related phenomena of long spin relaxation times in QD's (Refs. 1–5) and several investigations of their underlying mechanisms[6–10] have been reported in the literature. However, the underlying mechanism of Stokes shift is still far from clear. In the case of semiconductor QD's, this shift decreases with an increase in the radius of the dot and disappears beyond a certain radius. The redshift, principally, occurs if either the top of the valence band is an optically passive state (say, *P* state) or if the electron and hole are in a triplet state. Absorption of a photon from the top of the valence band in such cases is not allowed and is possible only from an optically active state lying deeper in the valence band. The exciton, once formed after absorption, cannot decay to the top of the valence band by a direct dipole transition and hence is called "dark exciton."[1] Deexcitation eventually takes place with the help of phonons, thus giving rise to redshifted photons.

In this paper we investigate the origin of Stokes shift in III-V(InAs) and II-VI(CdSe) semiconductor-based QD's. InAs and CdSe are chosen because of their (i) different crystal structures, (ii) different crystal-field effects which is zero in zinc-blende structures (i.e., InAs) but significantly large in wurtzite structure (CdSe), (iii) different effective masses which are small in InAs, but large for CdSe, and (iv) different nature of bonds. It has been observed experimentally[1,2,4] that the redshift decreases with radius and disappears beyond a certain radius. Essentially, the strong dependence of Stokes shift on the radius of the QD is used to investigate the origin of Stokes shift. The redshift calculated for different mechanisms is compared with the experimentally observed Stokes shift in QD's based on these semiconductors (InAs, CdSe). The redshift is obtained by calculating the energies of excitonic states taking into account the dielectric mismatch effects, the effect of finite barrier height, and the effect of the electron-hole exchange interaction.

II. MECHANISMS BEHIND THE STOKES SHIFT

Two different mechanisms[9,2] have been proposed to explain the origin of Stokes shift in semiconductor QD's, as shown in Fig. 1. Absorption takes place from the *S* state which lies deeper than the *P* state in the valence band to form an exciton in the singlet state of the electron and hole. According to the first mechanism, (1) of Fig. 1, deexcitation takes place into the *P* state with the help of phonons, giving rise to a Stokes shift by an amount ΔE_{SP} representing the difference in energy between the exciton states formed with *S* and *P* hole states (Ref. 9). According to the second mechanism the exciton in the singlet state first thermalizes into a triplet state from where it deexcites with the help of phonons either (a) to the deeper lying original *S* state, (2) of Fig. 1, giving rise to a Stokes shift by an amount ΔE_{ST} representing the singlet triplet splitting (Ref. 2), or (b) to the *P* state at the top of the valence band, (3) of Fig. 1, with the Stokes shift given by $\Delta E_{SP}+\Delta E_{ST}$. In addition to this, the redshift is also observed if the final excited state has a different atomic configuration than the initial ground state. Such a redshift, known as Frank-Condon shift, is commonly observed in molecules and point defects in solids and may be relevant in ultrasmall QD's.[11]

The possibilities of the different mechanisms can be understood by looking at the selection rules governing the optical transitions. The probabilities of the optical transition at the band edges in QD's are governed by the matrix element of the operator $e\hat{\mathbf{p}}$ between the states at the valence band top and the bottom of the conduction band, where $\hat{\mathbf{p}}$ is a momentum operator. Optical transitions from the electron state,[12]

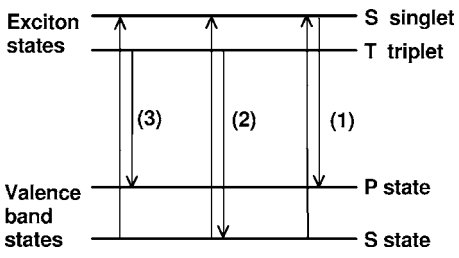

FIG. 1. The schematic representation of excitation-deexcitation processes taking place at the band edges.

$$\psi_e(\mathbf{r}) = j_0\left(\frac{\alpha_1^0}{R}r\right)Y_{00}(\theta,\phi)|S\alpha\rangle, \tag{1}$$

where $|S\alpha\rangle$ are the Bloch functions of the conduction band and α_1^0 is the first zero of $j_0(kr)$, are possible only to hole states in the valence band which have the S state as a component because $\int Y_{Lm}Y_{00}d\Omega = \delta_{L,o}\delta_{m,o}$. The optical transition probability from the bottom of the conduction band to a hole state in the valence band is given by[12] $P_{\alpha\beta} = |\int dr r^2 j_0\left(\frac{\alpha_1^0}{R}r\right)[cR_o(r)]|^2 |\langle u_\mu\beta|e\hat{\mathbf{p}}|S\alpha\rangle|^2$, where c is the component of the S state $R_o(r)$ in the hole wave function, β is the spin projection of the removed electron in the hole state, and u_μ are the Bloch wave functions of the hole states at the valence band top. $P_{\alpha\beta}$ is zero if $\alpha \neq \beta$. Optical transitions from the bottom of the conduction band to the top of the valence band are not possible if either (1) the hole state does not have a component of the S state (i.e., if $c=0$) or (2) the spin projections of the removed electron in the hole state and the electron in the conduction band are not equal, $\alpha \neq \beta$. Since the hole spin is obtained by flipping the spin of the removed electron, it follows that optical transitions are not possible if the spins of the electron and the hole are parallel—i.e., if they are in a triplet state. Thus, if the top of the valence band is a P state or the electron and hole are in a triplet state, a *dark exciton* is formed. In both cases the excitation takes place from a hole state having a S-state component, lying deeper in the valence band, to the electron S state in the conduction band (Fig. 1). This is a transition to a singlet state between the electron and hole which has higher energy than the triplet state. According to the first mechanism, deexcitation takes place eventually with the help of phonons to the P state at the top of the valence band, giving rise to a redshift between the emission spectra relative to the absorption spectra by an amount ΔE_{SP}. In the second case deexcitation takes place from the triplet state, reached by the thermalization, either to the P state at the top of the valence band or to the original S state lying deeper in the valence band with the help of phonons giving rise to the redshift $\Delta E_{SP}+\Delta E_{ST}$ and ΔE_{ST}, respectively.

III. EXCITONIC STATES IN SPHERICAL QUANTUM DOTS

The exciton states are obtained from the Hamiltonian

$$H = H_e + H_h + H_{so} + V_{e\text{-}h} + V_{Pol\text{-}s} + V_{Pol\text{-}eh}, \tag{2}$$

where H_e, H_h, H_{so}, and $V_{e\text{-}h}$ are the electronic Hamiltonian, the hole Hamiltonian, the spin-orbit interaction, and the e-h Coulomb interaction, respectively.[9,14] The last two terms represent the surface polarization energies arising due to the difference in the dielectric constants between the semiconductor quantum dot and the surrounding medium.[13] $V_{Pol\text{-}s}$ is the self-energy of the electron and hole due to their image charges, and $V_{Pol\text{-}eh}$ is the mutual interaction energy between the electron and hole via image charges. The excitonic states obtained from Eq. (2) will be split further due to the exchange interaction[2] H_{ex} between the electron and hole.

H_e is effectively the Hamiltonian of a "free" electron with effective mass m_e^* confined to a spherical dot of radius R. The lowest eigenfunction of H_e is given by Eq. (1). Since an electron created in a higher state of the conduction band will quickly cascade down to the lowest state, this state is the state of interest in exciton calculation. The $\mathbf{k}\cdot\mathbf{p}$ hole Hamiltonian H_h and the spin-orbit interaction H_{so} are given in Refs. 9 and 15 for wurtzite structures in the effective mass theory. The basis used is the direct product of Bloch wave functions at the valence band top with angular momentum $I=1$ and the spin eigenstates ($|I,I_z\rangle|S,S_z\rangle$):

$$|u_1\rangle = |1,1\rangle\left|\tfrac{1}{2},\tfrac{1}{2}\right\rangle, \quad |u_2\rangle = |1,0\rangle\left|\tfrac{1}{2},\tfrac{1}{2}\right\rangle, \quad |u_3\rangle = |1,-1\rangle\left|\tfrac{1}{2},\tfrac{1}{2}\right\rangle,$$

$$|u_4\rangle = |1,1\rangle\left|\tfrac{1}{2},-\tfrac{1}{2}\right\rangle, \quad |u_5\rangle = |1,0\rangle\left|\tfrac{1}{2},-\tfrac{1}{2}\right\rangle,$$

$$|u_6\rangle = |1,-1\rangle\left|\tfrac{1}{2},-\tfrac{1}{2}\right\rangle, \tag{3}$$

where $|1,1\rangle = -\frac{1}{\sqrt{2}}|X+\imath Y\rangle, |1,0\rangle = |Z\rangle$, and $|1,-1\rangle = \frac{1}{\sqrt{2}}|X-\imath Y\rangle$. The hole Hamiltonian in this basis with the energy reference as the top of the valence band is given by

$$H_h + H_{so} = \frac{1}{2m_0}\begin{pmatrix} P_1 & S & -T & 0 & 0 & 0 \\ S^* & P_3+2m_0\lambda & -S & -2\sqrt{2}m_0\lambda & 0 & 0 \\ -T^* & -S^* & P_1+4m_0\lambda & 0 & -2\sqrt{2}m_0\lambda & 0 \\ 0 & -2\sqrt{2}m_0\lambda & 0 & P_1+4m_0\lambda & S & -T \\ 0 & 0 & -2\sqrt{2}m_0\lambda & S^* & P_3+2m_0\lambda & -S \\ 0 & 0 & 0 & -T^* & -S^* & P_1 \end{pmatrix}, \tag{4}$$

where $\lambda = \frac{\Delta_{so}}{3}$, Δ_{so} being the splitting at the top of the valence band Γ due to the spin orbit interaction. $P_1 = \gamma_1 p^2 - \sqrt{\frac{2}{3}}\gamma_2 P_0^{(2)}$, $P_3 = \gamma_1' p^2 + \sqrt{\frac{2}{3}}\gamma_2' P_0^{(2)} + 2m_0\Delta_{cr}$, $T = \eta P_{-2}^{(2)} + \delta P_2^{(2)}$, $T^* = \eta P_2^{(2)} + \delta P_{-2}^{(2)}$, $S = \Lambda p_0 P_{-1}^{(1)} + \sqrt{2}\gamma_3' P_{-1}^{(2)}$, and $S^* = -\Lambda p_0 P_1^{(2)} - \sqrt{2}\gamma_3' P_1^{(2)}$ where $P^{(2)}$ and $P^{(1)}$ are second- and first-rank spherical tensors formed out of the components p_x, p_y, and p_z and Δ_{cr} is the crystal-field splitting energy. The parameters $\gamma_1, \gamma_2, \gamma_1', \gamma_2'$, etc., are related to effective mass

parameters $L,M,N,\ldots$ by the relations[9] $\gamma_1=\frac{1}{3}(L+M+N)$, $\gamma_2=\frac{1}{3}(L+M+N)$, $\gamma_3=\frac{1}{6}R$, $\gamma_1'=\frac{1}{3}(T+2S)$, $\gamma_2'=\frac{1}{6}(T-S)$, $\gamma_3'=\frac{1}{6}Q$, $\eta=\frac{1}{6}(L-M+R)$, and $\delta=\frac{1}{6}(L-M-R)$.

While the basic structure in wurtzite is hexagonal close packed (hcp), the basic structure in the zinc-blende case is face-centered cubic (fcc). In zinc-blende structure crystal-field effects are absent and the transition from the Hamiltonian H_h+H_{so} in the wurtzite case to the corresponding one in the zinc-blende case is easily obtained by putting $\Delta_{cr}=0$, $\Lambda=0$, $R=Q=N$, $S=M$, and $T=L$. Baldereschi and Lipari[16,17] have shown that for the zinc-blende structures the spherical symmetry approximation for the Hamiltonian is a good approximation.

The eigenfunction of the Hamiltonian given in Eq. (4) can be written as

$$\Psi_{m+1/2}=\sum_{\ell,n} C_{n,\ell} j_\ell(k_n^\ell r)\begin{pmatrix} a_{n,\ell}Y_\ell^{m-1}(\theta,\phi) \\ b_{n,\ell}Y_\ell^{m}(\theta,\phi) \\ d_{n,\ell}Y_\ell^{m+1}(\theta,\phi) \\ a'_{n,\ell}Y_\ell^{m}(\theta,\phi) \\ b'_{n,\ell}Y_\ell^{m+1}(\theta,\phi) \\ d'_{n,\ell}Y_\ell^{m+2}(\theta,\phi) \end{pmatrix}. \tag{5}$$

In Eq. (5), $j_\ell(x)$ is the spherical Bessel function, $k_n^\ell=\frac{\alpha_n^\ell}{R}$, where α_n^ℓ is the nth zero of $j_\ell(x)$, R is the dot radius, and $C_{n,\ell}$ is an overall normalization constant given by $C_{n,\ell}=\frac{\sqrt{2}}{R^{3/2}}\frac{1}{j_{\ell+1}(\alpha_n^\ell)}$. It should be noted that the ℓ_z values in the last three terms of the column matrix, given in Eq. (5), are one more than the corresponding values in the first three, because the former are associated with spin states with $S_z=\frac{1}{2}$ while the latter are associated with $S_z=-\frac{1}{2}$. Each eigenfunction is characterized by a definite value of $M=m+\frac{1}{2}=\ell_z+I_z+S_z$ where ℓ_z, I_z, and S_z represent the z components of the spherical harmonics, Bloch wave functions at the valence band top, and the spin part, respectively. The energy eigenvalues and wave functions for the hole states are obtained from the solution of the Schrödinger equation

$$H\Psi_{m+1/2}=E\Psi_{m+1/2}, \tag{6}$$

with H given by Eq. (4) and $\Psi_{m+1/2}$ given by Eq. (5).

The Coulomb interaction between the electron and hole V_{eh} is given by

$$V_{eh}=-\frac{e^2}{r_{eh}},$$

where $e(h)$ refers to the electron (hole). If we take the excitonic Bohr radius in the medium $a_{ex}=\hbar^2\epsilon_d/m_e^*e^2$ and Rydberg $R_{ex}=m_e^*e^4/2\hbar^2\epsilon_r^2$ (m_e^* is the effective mass of the electron in units of the free electron mass m_0, and ϵ_d is the dielectric constant of the dot material) as the units of length and energy, respectively, V_{eh} becomes

$$V_{eh}=-\frac{2}{r_{eh}}. \tag{7}$$

The exciton wave function can be expanded in terms of the electron and hole wave functions as

$$\psi_{ex}=\sum_{i,j} C_{ij}\psi_{ei}(\vec{r}_e)\psi_{hj}(\vec{r}_h), \tag{8}$$

where $\psi_{ei}(\vec{r}_e)$ is the eigenstate of the electron of the conduction band and $\psi_{hj}(\vec{r}_h)$ is the hole eigenstate obtained from Eq. (6). The exciton energy can be obtained from the secular equation

$$\left|(E_{n_e,l_e}+E_{m_h,l_h}-E)\delta_{ik}\delta_{jl}+V_{ij,kl}\right|=0, \tag{9}$$

where[9]

$$V_{ij,kl}=\left\langle \psi_{ei}(\vec{r}_e)\psi_{hj}(\vec{r}_h)\left|\frac{-2}{r_{eh}}\right|\psi_{ek}(\vec{r}_e)\psi_{hl}(\vec{r}_h)\right\rangle.$$

The effects due to the difference in the dielectric constant between the semiconductor quantum dot and the surrounding medium in the excitonic Hamiltonian are given by $V_{Pol\text{-}s}$ and $V_{Pol\text{-}eh}$. These two terms represent the surface polarization energies and are given by[13]

$$V_{Pol\text{-}s}=\frac{e^2}{2R}\sum_{n=0}^{\infty}\alpha_n\left[\left(\frac{r_e}{R}\right)^{2n}+\left(\frac{r_h}{R}\right)^{2n}\right],$$

$$V_{Pol\text{-}eh}=-\frac{e^2}{2R}\sum_{n=0}^{\infty}\alpha_n\left(\frac{r_e r_h}{R^2}\right)^n P_n(\cos\theta_{eh}), \tag{10}$$

where P_n is the Legendre polynomial of nth order and θ_{eh} is the angle between r_e and r_h. The dielectric constants of the semiconducting material of the dot and the surrounding medium are denoted by ϵ_d and ϵ_s, respectively, and α_n is defined by $\alpha_n=\frac{(n+1)(\epsilon-1)}{\epsilon_s(n\epsilon+n+1)}$ with $\epsilon=\frac{\epsilon_d}{\epsilon_s}$. Both $V_{Pol\text{-}s}$ and $V_{Pol\text{-}eh}$ become zero when either the radius of the dot $R\to\infty$ or $\epsilon=\frac{\epsilon_d}{\epsilon_s}=1$ ($\alpha_n=0$). Both cases correspond to no dielectric mismatch between the system and the surroundings.

In addition to the Coulomb interaction there is the exchange interaction[2,13] between the electron and hole which spilts the active exciton states described above and is given by

$$H_{ex}=\left(-\frac{2}{3}\right)\epsilon_{ex}(a_0)^3\delta(\vec{r}_e-\vec{r}_h)\sigma\mathbf{J}, \tag{11}$$

where ϵ_{ex} is the exchange strength constant, a_0 the lattice constant, σ the Pauli spin matrices representing the electron spin, and $\mathbf{J}$ the hole spin matrix. The exchange interaction was diagonalized in the eight dimensional basis[2,14] obtained by taking the direct product of the hole S states with $M=\pm\frac{3}{2}$ and $M=\pm\frac{1}{2}$ and the electron spin states $\pm\frac{1}{2}$.

IV. RESULTS AND DISCUSSION

The redshift of the emission spectra relative to the absorption spectra is observed if there is a formation of dark exciton at the band edge. As mentioned earlier a dark exciton is formed if either the top of the valence band is a P state or the electron at the bottom of the conduction band and the hole in the valence band are in a triplet state. In the first case the redshift is given by ΔE_{SP} (see Fig. 1) representing the differ-

ence in energy between the exciton states formed with optically active S-hole state and optically passive P-hole state. In the second case the redshift is given by the amount ΔE_{ST} representing the singlet-triplet splitting. In view of the different mechanisms involved, the discussion is divided into two subsections. In the first subsection we investigate the ΔE_{SP} mechanism by studying the nature of the state at the top of the valence band—i.e., whether the state is an optically passive P state or an optically active S state. In the second subsection we study the exchange interaction between the electron and hole which gives rise to a ΔE_{ST} splitting between the triplet and singlet states with the triplet state lying lower in energy.

A. Mechanism 1: Splitting= ΔE_{SP}

Since the nature of the state at the top of the valence band plays a pivotal role in the formation of dark and bright excitons, we first investigate the hole states for both the zinc-blende and wurtzite structures using the $\mathbf{k}\cdot\mathbf{p}$ hole Hamiltonian H_h+H_{so} given in Eq. (4). The energy eigenvalues of the hole states without inclusion of excitonic effects as a function of dot radius for InAs (zinc-blende structures) and CdSe (wurtzite structures) are shown in Figs. 2(a) and 3(a), respectively. These eigenvalues get modified when the Coulomb interaction between the electron in the conduction band and hole in the valence band is taken into account. The corresponding results including excitonic effects are shown in Figs. 2(b) and 3(b), respectively.

From Fig. 2(a) we observe that in InAs the optically passive $P_{3/2}$ is the ground state which lies below the first optically active state $S_{3/2}$ state. The states are labeled $S_{3/2}$, $P_{3/2}$ etc., where the capital letters correspond to the lowest $\mathbf{L}$ present and the subscripts gives the total angular momentum $\mathbf{F}'=\mathbf{L}+\mathbf{I}+\mathbf{S}$, where $\mathbf{L}$ is the orbital angular momentum, $\mathbf{I}(=1)$ is angular momentum of the Bloch wave function at the valence band top, and $\mathbf{S}$ is the spin of the hole. The states are degenerate with respect to the z component. The difference in energy between the optically passive $P_{3/2}$ state and the optically active $S_{3/2}$ state decreases as the radius of the dot increases and eventually $S_{3/2}$ becomes the ground state at around $R\sim 50$ Å. Hence dark-exciton formation and the associated Stokes shift will be observed below this radius.

Figure 3(a) gives the hole eigenvalues for the CdSe QD's with the wurtzite structure in the absence of an e-h interaction. The states are labeled as $|P_x\uparrow\rangle$, $|S_z\downarrow\rangle$, etc. Since the wurtzite Hamiltonian is axially symmetric, only the z component of the total angular momentum $\mathbf{F}'=\mathbf{L}+\mathbf{I}+\mathbf{S}$ is conserved. In labeling the states the capital letters (S, P, etc.) represent the dominant $\mathbf{L}$ present and the subscripts indicate whether the states are X, Y, or Z like, the arrow indicating the spin state. From Fig. 3(a) it is observed that for CdSe the optically passive $|P_x\uparrow\rangle$ with $M=\frac{1}{2}$ state is the ground state at $R\sim 10$ Å. The energy of $|P_x\uparrow\rangle$ in units of $\epsilon_0=\frac{\gamma_1}{2m_0}\left(\frac{\hbar}{R}\right)^2$ (γ_1 is a Luttinger parameter) has an upward slope as a function of radius and crosses the relatively flat $|S_x\uparrow\rangle$ state with $M=\frac{3}{2}$ at $R\sim 28$ Å. Dark-exciton formation and the Stokes shift are predicted for CdSe below $R\sim 28$ Å. The trend of S and P states can be explained by observing that $|S_x\uparrow\rangle$ with $M=\frac{3}{2}$ is

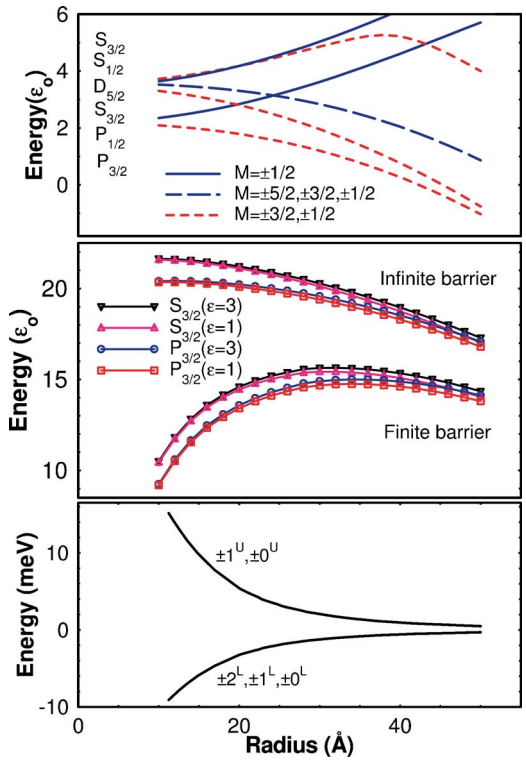

FIG. 2. (Color online) The energy levels in units of $\epsilon_0=\frac{\gamma_1}{2m_0}\left(\frac{\hbar}{R}\right)^2$ for zinc blende InAs QD's as a function of R in the (a) absence and (b) presence of an e-h Coulomb interaction (without exchange). The energy reference is taken as the top of the valence band without the spin-orbit effects included. Eigenvalues in the absence ($\epsilon=1$) as well as the presence ($\epsilon=3$) of dielectric mismatch effects are also shown in (b) for both the cases of infinite and finite barriers where $\epsilon=\frac{\epsilon_{dot}}{\epsilon_{surrounding}}$. (c) Eigenvalues including e-h Coulomb and exchange interactions. The states are labeled with F_z with superscripts standing for upper and lower states. The midpoint of the exciton energies with $M=\pm\frac{3}{2}$ and $M=\pm\frac{1}{2}$ is taken as the reference energy (zero of energy).

predominantly made from only one state with composition $L=0$, $I_z=+1$, $S_z=+\frac{1}{2}$ whose energy decreases as $\frac{1}{R^2}$ but in units of ϵ_0 is independent of R and hence the state is relatively flat.[14] But the optically passive P state with $M=\frac{1}{2}$ can be made either from the state with composition $L_z=-1$, $I_z=+1$, $S_z=+\frac{1}{2}(J_z=I_z+S_z=+\frac{3}{2})$ or the state with the composition $L_z=+1$, $I_z=-1$, $S_z=+\frac{1}{2}(J_z=-\frac{1}{2})$. These two states are separated from each other by a spin-orbit interaction. At very low radii spin-orbit effects are negligible relative to kinetic energy terms due to confinement. Hence the two states are almost degenerate at $R\sim 10$ Å. The coupling between these two states gives rise to a splitting of the states with the lower P state lying below the S state.[14] As the radius increases the energies of both the S and P states decrease. The energy of the S state decreases as $\frac{1}{R^2}$ but the energy of the P state decreases more slowly because of the presence of the spin-orbit interaction energy which becomes important as the kinetic energy starts decreasing with the increase of radius. Eventually the two levels cross. In Figs. 2 and 3 the energies are shown in units of ϵ_0.

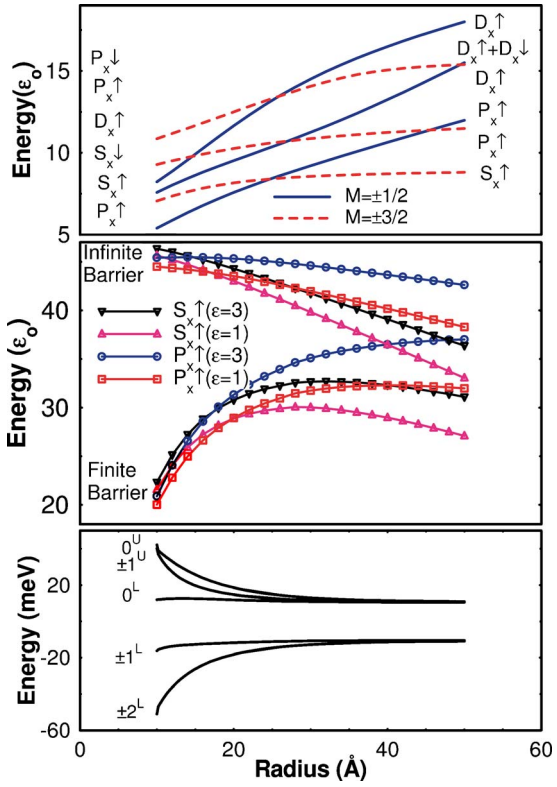

FIG. 3. (Color online) The energy levels in units of ϵ_0 for wurtzite CdSe QD's as a function of dot radius R in the (a) absence and (b) presence of an e-h Coulomb interaction and dielectric mismatch effects (without exchange) for both the cases of infinite and finite barriers. The energy reference is taken as the top of the valence band with the spin-orbit effects included. The states are labeled as $S_x\downarrow, P_x\uparrow$, etc., where capital letters represent the dominant **L** present and the subscripts stand for X-, Y-, or Z-like states, the arrow indicating the spin state. (c) Eigenvalues including e-h Coulomb and exchange interactions.

When the Coulomb interaction between the electron in the $1S_e$ state and the hole is taken into account, the energies decrease. The decrease in energy of the S state is more than that of the P state, the overlap between the $1S_e$ state and S state of the hole being greater. This causes the crossing between S and P states to occur at lower values of R as can be seen from a comparison of Figs. 2(b) and 3(b) with the corresponding Figs. 2(a) and 3(a). The differences between the excitonic S and P states ΔE_{SP} as a function of R are shown in the insets to Figs. 4 and 5.

The surface polarization charges arising due to the dielectric mismatch between the dot and the surroundings also affect the excitonic energies. The contributions of self-energy $V_{Pol\text{-}s}$ and attractive energy $V_{Pol\text{-}eh}$ are opposite in sign and comparable in magnitude.[18] Hence the dielectric mismatch effects are greatly reduced with the net effect being an increase in energy depending on the amount of dielectric mismatch between the dot and the surrounding. The increase in energy for the P state is more than that for the S state, resulting in a crossover to occur at a lower dot radius. This can be seen from Figs. 2(b) and 3(b) which gives a comparison between the zero and finite dielectric mismatches—i.e., $\epsilon=1$ and $\epsilon=3$. The self-energy of a charge confined to a spherical dielectric is minimum[19] at $r=0$. Since $\langle r^2\rangle$ for the P state is larger compared to that for the S state, the self-energy $V_{Pol\text{-}s}$ is higher for the P state. Moreover, the attractive energy $V_{Pol\text{-}eh}$ is higher for the S state compared to the P state. This also leads to a higher net increase of the polarization contribution $[V_{Pol\text{-}s}+V_{Pol\text{-}eh}]$ for the P state as compared to the S state and hence to a shifting of the S-P crossover to lower values of R as can be seen from Figs. 2(b) and 3(b).

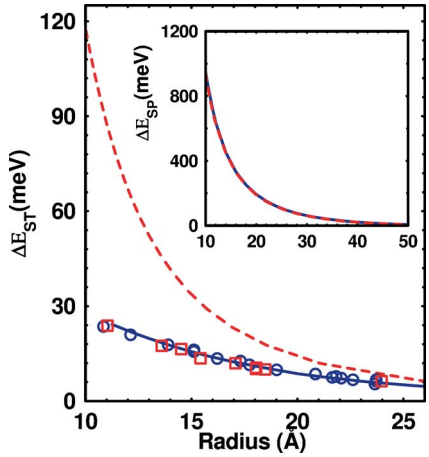

FIG. 4. (Color online) The singlet-triplet splitting in InAs for dielectric mismatch ratio $\epsilon=3$. The curves for no dielectric mismatch case $\epsilon=1$ superimpose on the curves for $\epsilon=3$. The solid line represents the finite-barrier case and the dashed line represents the infinite-barrier case. The inset gives the energy differences of S and P states. Experimental data (open circle and square) are taken from Ref. 4.

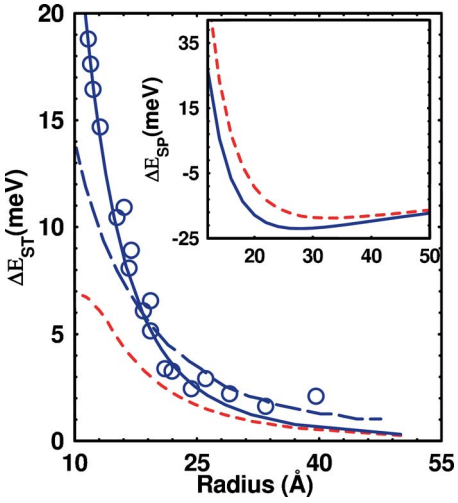

FIG. 5. (Color online) The singlet-triplet splitting in CdSe for dielectric mismatch ratio $\epsilon=3$. The curves for no dielectric mismatch case $\epsilon=1$ almost superimpose on the curves for 3 (Ref. 14). The solid line represents the results obtained by us for the case of an infinite barrier and the short dashed curve for the finite-barrier case. The long dashed curve represents the results obtained by Efros *et al.* for the infinite-barrier case. The inset gives the energy difference of S and P states with $M=\frac{3}{2}$ and $\frac{1}{2}$, respectively, for $\epsilon=3$. Experimental date (open circle) are taken from Ref. 2.

B. Mechanism 2: Splitting= ΔE_{ST}

Another cause of dark-exciton formation and the consequent Stokes shift is the splitting of the active exciton states due to the electron-hole exchange interaction.[2] The exchange interaction gives rise to a splitting between triplet and singlet states of the electron and hole, with the triplet state lying lower in energy. As seen from mechanism (2) of Fig. 1, the triplet state being passive, excitation takes place at the higher singlet state. Deexcitation can take place from the triplet state with the help of phonons or spin-flip assisted transitions, thus giving rise to a redshift of the emmision spectra with respect to the absorption spectra.

In InAs the first optically active S state [Fig. 2(a)] for the hole has total angular momentum $\mathbf{F}'=\frac{3}{2}(\mathbf{L}=0,\mathbf{I}=1,\mathbf{S}=\frac{1}{2})$ and is fourfold degenerate with respect to its z component $M=\pm\frac{3}{2},\pm\frac{1}{2}$. The $1S_e$ electron state in the conduction band being doubly degenerate, the exciton states are eightfold degenerate in the absence of exchange interaction. The exchange interaction splits these degenerate levels into two: the lower state with $\mathbf{F}=2(\mathbf{F}=\mathbf{F}'+\mathbf{S}_e)$ and the upper state with $\mathbf{F}=1$ [Fig. 2(c)]. Both the states are degenerate with respect to their z components. The $\vec{F}=2$ state is a triplet state. (The only way a state with total angular momentum 2 can be obtained from the electron and hole in the S state is by coupling the spins of the hole and electron to 1 and then coupling it with $I=1$.) Hence it is optically passive and forms a dark exciton. The upper state with $F=1$ is a singlet state. It is optically active and forms a bright exciton. The difference in energies ΔE_{ST} between the singlet and triplet states as a function of dot radius is shown in Fig. 4. ΔE_{ST} decreases with R and vanishes at $R\sim 35$ Å. The exchange interaction is enhanced with a decrease in radius because of the increase in the overlap of electron and hole wave functions due to confinement.

In CdSe [Fig. 3(c)] the ground state with $F_z=\pm 2$ can be obtained by coupling a hole with $M=\pm\frac{3}{2}$ with the electron state with $(S_e)_z=\pm\frac{1}{2}$. Since these combinations form triplet states, the ground state with $F_z=\pm 2$ is optically passive and forms a dark exciton. The first excited state with $F_z=\pm 1^L$ can be obtained either by coupling $M=\pm\frac{3}{2}$ with $(S_e)_z=\mp\frac{1}{2}$ or alternatively by $M=\pm\frac{1}{2}$ with $(S_e)_z=\pm\frac{1}{2}$. The state $\pm 1^L$ will be a mixture of singlet and triplet states and will be optically active. The difference in energies ΔE_{ST} between the optically passive ground state and the first optically active excited state as function of R for CdSe is shown in Fig. 5. As in the case of InAs, ΔE_{ST} for CdSe also decreases with R and vanishes around $R\sim 50$ Å.

As seen from Figs. 2–5 the curves corresponding to the finite-barrier case lie lower than infinite-barrier case. This is due to the penetration of a substantial amount of electron wave function outside the dot, giving rise to a lower eigenvalue of the electron wave function. Moreover, both the exchange interaction and Coulomb interaction which depend on the amount of overlap of electron and hole wave functions are also reduced in the finite-barrier case, resulting in decrease of the exchange energy and Coulomb binding energy.

Having theoretically calculated ΔE_{SP} and ΔE_{ST} we are in a position to investigate the various mechanisms for Stokes shift given in Fig. 1 by comparison with experimental data. In Figs. 4 and 5 are shown the plots of ΔE_{ST} as a function of the dot radius together with the experimentally observed Stokes shift for InAs and CdSe, respectively. ΔE_{SP} as a function of R for these cases is shown in the insets of the corresponding figures. It is observed that ΔE_{SP} is much larger than the experimental redshift for InAs. For CdSe, as seen from the inset of Fig. 5, at $R\sim 13$ Å, ΔE_{SP} is almost the same as the experimental Stokes shift but for larger values of R the experimental values are much higher. It is seen from Figs. 4 and 5 that ΔE_{ST} fits the experimental data rather well. We observed that the fit for CdSe corresponds to an infinite barrier at the dot radius but for InAs a good fit is obtained for a finite-barrier height. This can be explained by observing that the effective mass of electron in InAs is very small and hence the lowest eigenvalue lies near the top of the barrier height and there is substantial probability of finding the electron outside the dot. For CdSe, the effective mass of electron is large and the lowest eigenvalue lies near the bottom of the potential well, making the infinite-barrier effects predominant. In Fig. 5 we have also plotted the theoretical curve for Stokes shift obtained by Efros *et al.*[2] in which the Coulomb interaction between the electron and hole was not taken into account. We observe that better agreement with experimental Stokes shift is obtained by our theoretical curve which takes into account the Coulomb interaction.

V. CONCLUSIONS

From a comparison of the theoretical results with experimental data we conclude that the Stokes shift observed in QD's is caused by a splitting of the exciton states by the electron-hole exchange interaction through the deexcitation mechanism (2) in Fig. 1, which takes into account the Coulomb interaction and the effects of dielectric mismatch.

[1] M. Nirmal, D. J. Norris, M. Kuno, M. G. Bawendi, Al. L. Efros, and M. Rosen, Phys. Rev. Lett. **75**, 3728 (1995).
[2] Al. L. Efros, M. Rosen, M. Kuno, M. Nirmal, D. J. Norris, and M. G. Bawendi, Phys. Rev. B **54**, 4843 (1996).
[3] M. Paillard, X. Marie, P. Renucci, T. Amand, A. Jbeli, and J. M. Gerard, Phys. Rev. Lett. **86**, 1634 (2001).
[4] U. Banin, J. C. Lee, A. A. Guzelian, A. V. Kadavanich, and A. P. Alivisatos, Superlattices Microstruct. **22**, 559 (1997).
[5] A. Tackeuchi, R. Ohtsubo, K. Yamaguchi, M. Murayama, T. Kitamura, T. Kuroda, and T. Takagahara, Appl. Phys. Lett. **84**, 3576 (2004).
[6] P. D. J. Calcott, K. J. Nash, L. T. Canham, M. J. Kane, and D. Brumhead, J. Phys.: Condens. Matter **5**, L91 (1993).
[7] P. D. J. Calcott, K. J. Nash, L. T. Canham, M. J. Kane, and D.

Brumhead, J. Lumin. **57**, 257 (1993); **60&61**, 297 (1994).
[8] K. Leung and K. B. Whaley, Phys. Rev. B **56**, 7455 (1997).
[9] J. Li and J. B. Xia, Phys. Rev. B **61**, 15880 (2000).
[10] T. Bakos, S. N. Rashkeev, and S. T. Pantelides, Phys. Rev. Lett. **91**, 226402 (2003).
[11] A. Franceschetti and S. T. Pantelides, Phys. Rev. B **68**, 033313 (2003).
[12] Al. L. Efros, Phys. Rev. B **46**, 7448 (1992).
[13] T. Takagahara, Phys. Rev. B **47**, 4569 (1993).
[14] A. Bagga, P. K. Chattopadhyay, and S. Ghosh, Phys. Rev. B **71**, 115327 (2005).
[15] A. Bagga, P. K. Chattopadhyay, and S. Ghosh, Phys. Rev. B **68**, 155331 (2003).
[16] J. B. Xia, J. Lumin. **70**, 120 (1996).
[17] A. Baldereschi and N. O. Lipari, Phys. Rev. B **8**, 2697 (1973).
[18] V. A. Fonoberov, E. P. Pokatilov, and A. A. Balandin, Phys. Rev. B **66**, 085310 (2002).
[19] L. E. Brus, J. Chem. Phys. **79**, 5566 (1983).